ChemComm

Accepted Manuscript

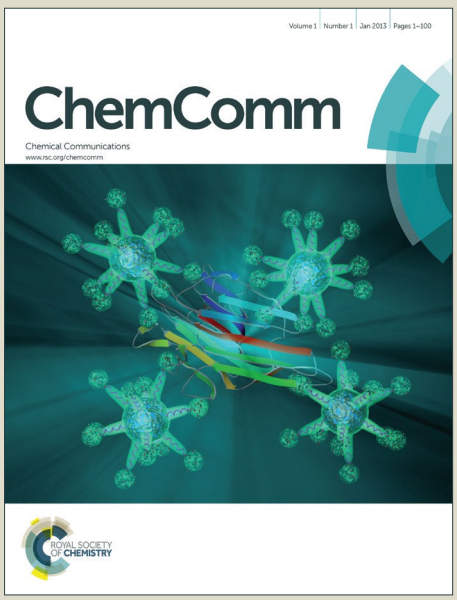

ROYAL SOCIETY OF CHEMISTRY

www.rsc.org/chemcomm

Journal Name

RSCPublishing

COMMUNICATION

Efficient charge separation on 3D architectures of TiO_2 mesocrystals packed with chemically exfoliated MoS_2 shell in synergetic hydrogen evolution

Cite this: DOI: 10.1039/xoxxoooooox

Received ooth January 2012,
Accepted ooth January 2012

DOI: 10.1039/xoxxoooooox

www.rsc.org/

Peng Zhang,[a] Takashi Tachikawa,[b]* Mamoru Fujitsuka[a] and Tetsuro Majima[a]*

Here we demonstrated that 3D architectures of TiO_2 mesocrystals uniformly packed with a chemically exfoliated MoS_2 shell exhibit promising reactive efficiency and good stability in the synergetic hydrogen evolution. The efficient interfacial electron transfer from the excited TiO_2 moieties to decorated ultrathin MoS_2 shell was effectively monitored.

With mounting concern regarding the reduction of human energy usage and alleviating environmental issues, the efficient utilization of solar energy has become a major research interest over the past few decades. Hydrogen as a renewable resource has been studied extensively in this regard,[1] with photocatalysis playing an important role in applications of solar-driven hydrogen evolution since the 1970s.[2] For example, TiO_2 photocatalysts have attracted a great amount of research interest in terms of the hydrogen evolution reaction (HER) because of their strong redox ability, high chemical stability, low toxicity, and abundant availability.[3] However, TiO_2 itself showed a poor HER activity even in the presence of sacrificial reagents. In order to promote the HER, robust cocatalysts are usually present on semiconductor materials as active sites.[4] Among the noble metals, platinum (Pt) nanoparticles exhibited an efficient HER due to the ideal free energy of hydrogen adsorption.[5] However, the high price and insufficient storage of Pt limit its application in commercial production. Thus, the development of a cocatalyst with low cost and good performance in the HER is strongly motivated in regards to both scientific and engineering interests.

Recently, two-dimensional MoS_2 nanosheets have been extensively investigated and considered as an alternative candidate for the replacement of Pt in efficient HERs.[6] MoS_2 nanosheets coupled with semiconductor nanoparticles such as TiO_2 have been synthesized and shown higher activity in the HER than MoS_2 or TiO_2 alone.[7] MoS_2 forms two different crystal structures: an octahedral (1T) phase and a trigonal prismatic (2H) phase. The metallic 1T-MoS_2 showed higher HER rates because of its higher conductivity; however, it was observed that this phase was not thermally stable.[8] The increase in the number of active sulfur edge sites on 2H-MoS_2, in preference to inert basal planes, has become essential in the improvement of the reaction efficiency.[9] However, semiconducting 2H-MoS_2 is generally combined with additive photosensitizers[10] or conductive materials[11] to overcome the inherent restriction of poor electrical conductivity. However, the irregular restacking of MoS_2 layers, which potentially reduces the number of active sites, and complicated synthetic procedures (e.g., introduction of graphene as a third component) are disadvantageous for their implementation in practical applications. We thus conclude that both the photoconductivity and the photocatalytic activity of supporting semiconductor materials are essential for achieving the desired functionality.

In the development of a new class of porous materials, we have recently demonstrated that anatase TiO_2 mesocrystals (TMCs) significantly enhance the charge separation with remarkably long-lived charges (over 4 times), and exhibit excellent photoconductivity (over 10 times) than nanocrystal samples, and even similar photocatalytic activities for organic degradation as commercial P25, which is a benchmark TiO_2 photocatalyst.[12] TMCs consist of TiO_2 nanocrystal building blocks and form a well-defined crystal shape. Herein we report a new synthetic approach involving the assembly of chemically exfoliated MoS_2 shell as cocatalysts packed on external surfaces of TMCs after mild impregnation and annealing. The synergetic HER of MoS_2 shell with maximum active sites supported on TMCs (MoS_2/TMC) exhibited higher activity than in a nanoparticle-based system using P25. It was further revealed by time-resolved diffuse reflectance (TDR) spectroscopy that the higher HER efficiency was promoted by efficient charge separation and

[a]The Institute of Scientific and Industrial Research (SANKEN), Osaka University, Mihogaoka 8-1, Ibaraki, Osaka 567-0047, Japan. Fax: +81-6-6879-8499; Tel: +81-6-6879-8495; E-mail: majima@sanken.osaka-u.ac.jp.

[b]Department of Chemistry, Graduate School of Science, Kobe University, 1−1 Rokkodai-cho, Nada-ku, Kobe 657−8501, Japan, and PRESTO, Japan, and Science and Technology Agency (JST), 4-1-8 Honcho Kawaguchi, Saitama 332-0012, Japan. Fax: +81-78-803-5736; Tel: +81-78-803-5736; Email: tachikawa@port.kobe-u.ac.jp.

†Electronic Supplementary Information (ESI) available: [details of any supplementary information available should be included here]. See DOI: 10.1039/c000000x/

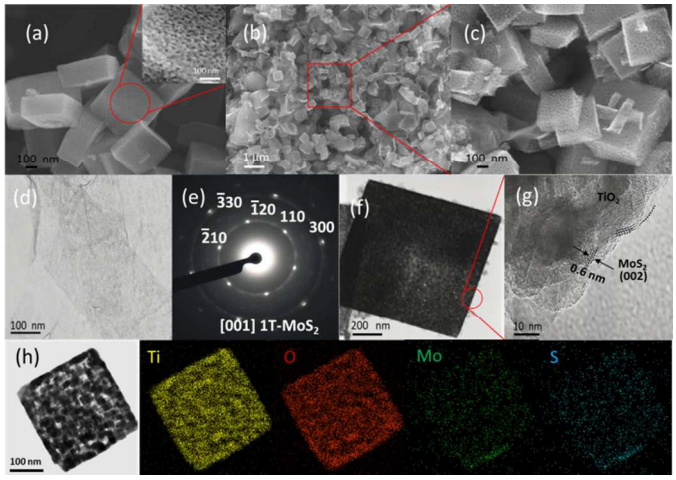

Fig. 1 FESEM images of (a) TMC, (b) MoS_2/TMC, and (c) magnified image of panel b. The inset of panel (a) is the magnified image. TEM image of (d) MoS_2 and its (e) SAED; and (f) MoS_2/TMC and its (g) HRTEM. (h) Bright-field STEM image (leftmost image) and STEM-EDS elemental mapping images of MoS_2/TMC.

interfacial electron transfer in MoS_2/TMC. The 3D architectures of MoS_2/TMC with promising superiority are expected to become a potential competitor to earth-abundant catalysts for the HER.

The general morphologies of the materials (see Supporting Information for synthetic procedures) were characterized by field-emission scanning electron microscopy (FESEM) and transmission electron microscopy (TEM). In Fig. 1a, it can be seen that the TMCs, which were newly synthesized via topotactic conversion from precursor NH_4TiOF_3 crystals,[12a] display cubic-like morphologies. We also observed that TMCs with porous structures were composed of an ordered alignment of anatase TiO_2 nanocrystals, with sizes of ~20 nm, as determined from the magnified FESEM image of the crystal surface (insert in Fig. 1a) and from the TEM image (Fig. S1a, ESI†).

The basal and lateral surfaces were found to mainly correspond to the {001} and {101} facets, respectively, as can be deduced from the selected-area electron diffraction (SAED) pattern as shown in Fig. S1a (ESI†). The uniform superstructures with an average of ~220 nm thickness and ~500 nm size (Fig. S1b, ESI†) can be successfully implemented as the platform for size-matching MoS_2 nanosheets (see below). The FESEM images of the MoS_2/TMC (Figs. 1b and 1c) indicate that the structure of the TMCs remains intact after the modification treatment, and the majority of MoS_2 nanosheets are uniformly attached onto the external surfaces of TMCs without considerable aggregation. The detailed structures of MoS_2 nanosheets and 3D architectures of MoS_2/TMC were further examined. Fig. 1d shows that the chemically exfoliated MoS_2 moieties are nearly transparent sheets with partial overlaps. By atomic force microscopy (AFM), the size and thickness of the MoS_2 monolayer were found to be ~400 nm and ~1.6 nm, respectively (Fig. S3, ESI†).[13] The SAED pattern recorded on exfoliated MoS_2 exhibits a diffraction pattern corresponding to 1T-MoS_2 along the [001] zone axis (Fig. 1e).[8a,b] Fig. 1f shows the TEM image of MoS_2/TMC. The high-resolution TEM (HRTEM) analysis clearly reveals that a layered MoS_2 exists at the lateral surface of TMC (Fig. 1g). The lattice spacing, as indicated by two dotted lines in Fig. 1g, was found to be approximately 0.62 nm, thus corresponding to the (002) plane of 2H-MoS_2.[11c] Furthermore, a number of folded edges exhibit multi-parallel lines corresponding to two or three layers of MoS_2. To confirm the spatial location of MoS_2 nanosheets on TMCs, elemental mapping was carried out using scanning TEM equipped with scanning TEM-energy dispersive X-ray spectroscopy (STEM-EDS) (Figs. 1h and S2, ESI†). From the top and side views of MoS_2/TMC, it can be suggested that MoS_2 nanosheets are homogeneously adsorbed on the exposed facets of TMCs, resulting in a shell around the TMC. Their intimate packing with maximizing active sites from large contact area creates a perfect electrical interface for charge transport. The EDS analysis proves the distribution of Mo (3.6 wt%) and S (5.2 wt%) on TMCs, which are consistent with the results of inductively coupled plasma (ICP) analysis.

The phase identities of the samples were collected using powder X-ray diffraction (XRD), as shown in Fig. 2a. The patterns of all TMCs were comparable with the standard peaks of the anatase phase. For stacked MoS_2 nanosheets on the glass substrate, a detectable diffraction peak was observed at 14.4°, which corresponds to the *c*-plane of stacking MoS_2.[8b] The patterns of MoS_2/TMC powders were also characterized and in accordance with each component. The intensities of (002), (100), and (110) diffraction peaks from MoS_2 increased gradually upon increasing the amounts of MoS_2 on the TMCs from 1 wt% to 23 wt%, as shown in Fig. S4a (ESI†). The nitrogen adsorption-desorption isotherms and the corresponding pore size distribution curves were used to investigate the textural properties of MoS_2, TMC, and MoS_2/TMC (Fig. S5, ESI†). The surface areas of TMC and MoS_2/TMC were calculated to be 62 $m^2 g^{-1}$ and 43 $m^2 g^{-1}$, respectively, with a similar mean pores size of ~24 nm (Table S1, ESI†). After the introduction of MoS_2, there was the slight decrease in surface area due to the presence of partially covered pores on the TMCs.

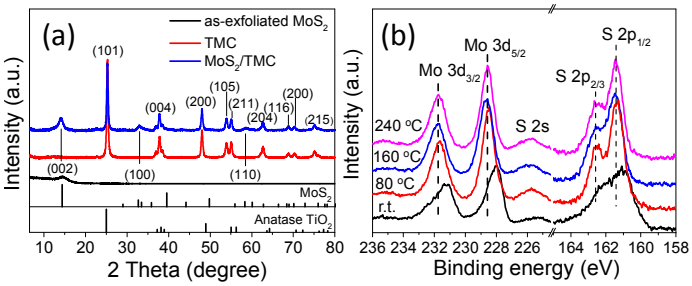

Fig. 2 (a) XRD patterns of MoS_2, TMC, and MoS_2/TMC (10 wt% MoS_2). (b) XPS spectra of MoS_2/TMC (10 wt% MoS_2) powders annealed at a range of temperatures.

X-ray photoelectron spectroscopy (XPS) was employed to investigate the phase composition of MoS_2 on TMCs at various annealing temperatures (Fig. 2b). At room temperature, the MoS_2/TMC showed binding energies of Mo $3d_{3/2}$, Mo $3d_{5/2}$, S $2p_{1/2}$, and S $2p_{3/2}$ at 231.2, 228.0, 162.1, and 161.0 eV, respectively.[8a] Upon elevating the annealing temperature, the binding energies of Mo 3d and S 2p shifted to higher energies, indicating a phase transition from 1T to 2H (see Fig. S6, ESI†),[8a] while no difference was observed in Ti 2p and O 1s for the TMCs due to the thermal stability at 500 °C (Fig. S7, ESI†).

The photocatalytic HER was evaluated on MoS_2 (exfoliated MoS_2 and MoS_2/Al_2O_3 annealed at 160 °C), TMC, and a range of MoS_2/TiO_2 with equal MoS_2 loadings (10 wt%), except in the case of pure TMC. The HER was investigated under UV light irradiation, where lactic acid was used as both a hole scavenger and as an abundant source of H^+ ions (Fig. 3a).[11d] A negligible amount of H_2 gas evolution was detected on MoS_2 or TMCs alone. Subsequently, a promising and synergetic improvement in the photocatalytic HER was observed on MoS_2/TMC, with the MoS_2 loading being found to

play a crucial role in the HER efficiency (Fig. S4b, ESI†). Even only 1 wt % of MoS_2 was loaded on TMC, the rate of HER increased up to 200 times, as compared with pure TMC. With the increase in the loading amounts of MoS_2 to less than 10 wt%, the rate of HER gradually increased due to an increase in the number of active sites from MoS_2 nanosheets. The highest HER rate (0.55 mmol h^{-1} g^{-1}) was obtained at an optimal value of 10 wt%, where the external facets of TMCs are mostly covered by MoS_2 nanosheets with providing maximum active sites (Fig. 1h and Supplementary calculation part). However, the excessive loading lowered the efficiency, possibly due to the competitive absorption of UV light from thick MoS_2 shell, and the interfacial barrier from stacking MoS_2 monolayers.[14]

We also observed that the HER over MoS_2/TMC was influenced by the annealing temperature, as demonstrated in Fig. S8 (ESI†). The photocatalysts exhibited the highest activity after annealing at a temperature of 160 °C. It is well-known that the phases of MoS_2 strongly affect the HER efficiency.[8e] As evidenced by XPS analysis, the MoS_2 phase changes from a mixture of 1T (60%) and 2H (40%) at room temperature, to almost pure 2H (92%) after annealing at 160 °C (Fig. S6 and Table S2, ESI†). A similar trend was observed elsewhere.[8a] At lower temperatures, a poor physical contact between MoS_2 and TMC resulted, which is disadvantageous to interfacial electron transfer, even though metallic 1T-MoS_2 has a better electrical conductivity.[8b] The decrease in activity after annealing at 240 °C may be attributed to the disappearance of the 1T phase and/or partial oxidation of active edge sites.[7b]

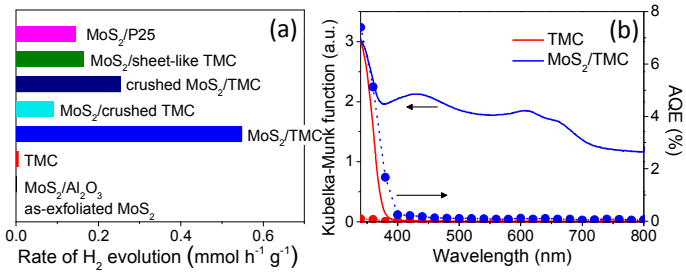

Fig. 3 (a) Comparison of the hydrogen generation rates of different samples. (b) Steady-state diffuse reflectance spectra (left axis, solid lines) and AQE (right axis, symbols with dashed lines) of TMC (red) and MoS_2/TMC (blue).

Under the same conditions, the optimal MoS_2/TMC gives an H_2 evolution rate of 0.55 mmol h^{-1} g^{-1}, which is 4 times greater than that of MoS_2/P25 (0.14 mmol h^{-1} g^{-1}), despite its larger surface area of 51 m^2 g^{-1} (Fig, S9a and Table S1, ESI†). To confirm the impact of mesocrystalline superstructures on the HER, we prepared two reference samples, crushed MoS_2/TMC and MoS_2/crushed TMC; in the latter case, TMCs were crushed by grinding with a mortar before modification (Fig. S9b, ESI†). As summarized in Fig. 3a, these composites exhibited much lower activity than MoS_2/TMC. The well-aligned nanocrystals on the external surfaces of TMCs form a close contact with the MoS_2 nanosheets without considerable aggregation, thus increasing active sites and facilitating the interfacial electron transfer to efficiently promote the HER. Furthermore, a unique morphological effect was observed; MoS_2/cubic-like TMC appears to be more active than MoS_2/sheet-like TMC (Fig. S9c, ESI†). This is likely due to the fact that the lateral surfaces of cubic-like TMCs are dominated by {101} facets, which are in favor of H_2 generation compared to the basal {001} surfaces of sheet-like TMCs.[15]

The apparent quantum efficiency (AQE) at each centered wavelength of the monochromatic light was calculated using the following equation: *AQE = (2 × number of H_2 molecules/number of incident photons) × 100%.* Results are shown in Fig. 3b for the UV-visible steady-state diffuse reflectance spectra of the samples tested (see Fig. S10 for the spectra of other samples, ESI†). The pure TMCs showed negligible H_2 generation in the whole wavelength region tested, due to their intrinsic limitation. On the other hand, MoS_2/TMC evolved H_2 gas, and the action spectrum of AQE was found to be in agreement with the absorption spectrum of TMCs. The AQE reached up to 7.4% at 340 nm and 5.1% at 360 nm. The obtained AQEs are slightly lower than 9.7% in MoS_2/TiO_2/reduced graphene oxide (RGO),[11b] although a simple comparison is difficult because of the different experimental conditions (Table S3, ESI†). Even though 2H-MoS_2 has an intrinsic visible light absorption, the MoS_2/TMC combination exhibits a poor visible performance due to insufficient charge generation from the excited MoS_2.[7c] The stability of MoS_2/TMC was further tested by recycling the catalyst for five times (Fig. S11, ESI†). After 25 h, the catalyst did not show any loss of the activity, indicating its reusability in the photocatalytic reactions.

To confirm the fast interfacial electron transfer dynamics around band aliment within the 3D architectures of MoS_2/TMC (Fig. S12, ESI†), we employed femtosecond TDR spectroscopy.[12b] After 330-nm laser excitation of MoS_2/TMC in ambient air, as shown in Fig. 4a, a broad absorption band appeared in the near-infrared region, which was superimposed with trapped and free (or shallowly trapped) electrons in TMCs.[12b] Similar absorption spectra were observed for pure TMC, P25, and MoS_2/P25 (Fig. S13, ESI†). In the period of 0–10 ps, the transient absorption decayed rapidly when compared with pure TMCs (black lines in Fig. 4b). After 10 ps had passed, the transient absorption diminished gradually. To evaluate the decay kinetics, the time profiles of absorption probed at 900 nm, were fitted using multi-exponential functions (Fig. 4b), and their lifetimes summarized in Table 1. By modifying TMCs with MoS_2, the lifetimes of the electrons were found to decrease largely to 1.7 ps (49%), 33 ps (32%), and 780 ps (19%) from corresponding time scales of 4.8 ps (23%), 53 ps (41%), and 1070 ps (36%) for pure TMCs. Considering that the transient absorption signal from MoS_2/Al_2O_3 is very weak and decays within 1 ps (Fig. S13b, ESI†), it was obvious that interfacial electron transfer could take place between TMCs and MoS_2. The reaction time of electrons was tentatively estimated using the diffusion coefficient of electrons in TiO_2 (Fig. S14 and Table S4, ESI†). The mean times required for electron diffusion from a nanocrystal (21 nm × 17 nm) to the neighboring MoS_2 were within tens of picoseconds, which is reasonably consistent with the first (τ_1) and second (τ_2) components. The third component (τ_3) of MoS_2/TMC is possibly mediated by multiple TiO_2 nanocrystals. The interparticle electron transfer over several hundred nanometers, which corresponds to more than ten nanocrystals, was expected to occur in the microsecond time scale,

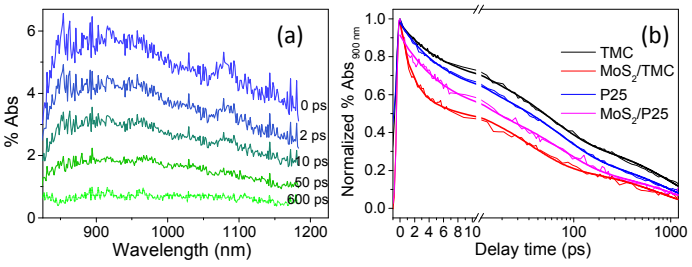

Fig. 4 Time-resolved diffuse reflectance spectra of MoS_2/TMC. (b) Normalized transient absorption traces observed at 900 nm for a range of samples. Bold lines indicate multiexponential curves fitted to kinetic traces.

Table 1 Kinetic parameters of transient absorption decays

Sample	τ_1 (ps)	τ_2 (ps)	τ_3 (ps)
MT	5.0 ± 0.4	55 ± 3	1100 ± 37 (33%)
MoS_2/MT	1.9 ± 0.1	36 ± 2	805 ± 53 (13%)
P25	6.0 ± 0.3	72 ± 4	1024 ± 46 (25%)
MoS_2/P25	7.6 ± 0.6	91 ± 12	1372 ± 271

which is beyond the time window measured here. It is noteworthy that MoS_2/P25 exhibits similar decay times to those of pure P25, except for the fast decay within ~1 ps (~10%), which might be indicative of electron transfer at the interface between TiO_2 and MoS_2. Thus, the well-ordered geometry of TMCs facilitates electron transfer between nanocrystals, resulting in the retardation of the charge recombination, and in efficient electron harvesting by MoS_2. This is likely to be the main reason why MoS_2/TMC exhibits a higher photocatalytic activity (2~5 times) compared to other MoS_2/TiO_2.

In summary, we decorated the newly designed TMCs packed with the chemically exfoliated MoS_2 shell by a simple impregnation method. MoS_2/TMC with maximum active sites from MoS_2 shell exhibits the high HER rate (0.55 mmol h^{-1} g^{-1}), high AQE (7.4%), and good reusability (over 25 h) under UV light irradiation, without conductive supports such as RGO. To verify the efficient charge separation in MoS_2/TMC, the electron transfer dynamics from the excited TMC to MoS_2 was directly monitored by transient absorption for the first time. Our strategy possesses not only a possibility for use of noble-metal-free MoS_2, but also confirms the crucial concept that the hetero-superstructure with the synergy is beneficial for achieving a high photocatalytic activity. It is believed that this approach can be exploited for a range of applications, such as (photo)catalysis, optoelectronics, and energy storage.

This work has been partly supported by Innovative Project for Advanced Instruments, Renovation Center of Instruments for Science Education and Technology, Osaka University, and a Grant-in-Aid for Scientific Research (Project 25220806, 25288035, 25810114, and others) from the Ministry of Education, Culture, Sports, Science and Technology (MEXT) of the Japanese Government. We are thankful for the help of the Comprehensive Analysis Center of SANKEN, Osaka University.

Notes and references

1. (a) X. Chen, S. Shen, L. Guo, S. S. Mao, *Chem. Rev.* 2010**, 110**, 6503; (b) A. Kudo, Y. Miseki, *Chem. Soc. Rev.* 2009, **38**, 253.
2. A. Fujishima, K. Honda, *Nature* 1972, **238**, 37.
3. (a) Y. Ma, X. Wang, Y. Jia, X. Chen, H. Han, C. Li, *Chem. Rev.* 2014, **114**, 9987; (b) M. Kapilashrami, Y. Zhang, Y. S. Liu, A. Hagfeldt, J. Guo, *Chem. Rev.* 2014, **114**, 9662; (c) L. X. Sang, Y. X. Zhao, C. Burda, *Chem. Rev.* 2014, **114**, 9283.
4. (a) J. Yang, D. Wang, H. Han, C, Li, *Acc. Chem. Res.* 2013, **46**, 1900; (b) J. Ran, J. Zhang, J. Yu, M. Jaroniec, S. Qiao, *Chem. Soc. Rev.* 2014, **43**, 7787; (c) X. Li, J. Yu, J. Low, Y. Fang, J. Xiao, X. Chen, *J. Mater. Chem. A* 2013, **3**, 2485.
5. (a) S. Trasatti, *J. Electroanal. Chem.* 1972, **39**, 163; (b) J. K. Nørskov, T. Bligaard, A. Logadottir, J. R. Kitchin, J. G. Chen, S. Pandelov, U. Stimming, *J. Electrochem. Chem.* 2005, **152**, 23; (c) J. K. Nørskov, T. Bligaard, J. Rossmeisl, C. H. Christensen, *Nat. Chem.* 2009, **1**, 37.
6. (a) M. Chhowalla, H. S. Shin, G. Eda, L. J. Li, K. P. Loh, H. Zhang, *Nat. Chem.* 2013, **5**, 263; (b) Y. Yan, B. Xia, Z. Xu, X. Wang, *ACS Catal.* 2014, **4**, 1693.
7. (a) S. Kanda, T. Akita, M. Fujishima, H. Tada, *J. Colloid Interface Sci.* 2011, **354**, 607; (b) W. Zhou, Z. Yin, Y. Du, X. Huang, Z. Zeng, Z. Fan, H. Liu, J. Wang, H. Zhang, *Small* 2013, **9**, 140; (c) L. A. King, W. Zhao, M. Chhowalla, D. J. Riley, G. Eda, *J. Mater. Chem. A* 2013, **1**, 8935; (d) C. Liu, L. Wang, Y. Tang, S. Luo, Y. Liu, S. Zhang, Y. Zeng, Y. Xu, *Appl. Catal., B*, 2015, **164**, 1.
8. (a) G. Eda, H. Yamaguchi, D. Voiry, T. Fujita, M. Chen, M. Chhowalla, *Nano Lett.* 2011, **11**, 5111; (b) M. A. Lukowski, A. S. Daniel, F. Meng, A. Forticaux, L. Li, S. Jin, *J. Am. Chem. Soc.* 2013, **135**, 10274; (c) Q. Ding, F. Meng, C. R. English, M. Cabán-Acevedo, M. J. Shearer, D. Liang, A. S. Daniel, R. J. Hamers, S. Jin, *J. Am. Chem. Soc.* 2014, **136**, 8504; (d) D. Voiry, M. Salehi, R. Silva, T. Fujita, M. Chen, T. Asefa, V. B. Shenoy, G. Eda, M. Chhowalla, *Nano Lett.* 2014, **13**, 6222; (e) U. Maitra, U. Gupta, M. De, R. Datta, A. Govindaraj, C. N. R. Rao, *Angew. Chem., Int. Ed.* 2013, **52**, 13057.
9. (a) B. Hinnemann, P. G. Moses, J. Bonde, K. P. Jørgensen, J. H. Nielsen, S. Horch, I. Chorkendorff, J. K. Nørskov, *J. Am. Chem. Soc.* 2005, **127**, 5308; (b) T. F. Jaramillo, K. P. Jørgensen, J. Bonde, J. H. Nielsen, S. Horch, I. Chorkendorff, *Science* 2007, **317**, 100; (c) J. Kibsgaard, Z. Chen, B. N. Reinecke, T. F. Jaramillo, *Nat. Mater.* 2012, **11**, 963.
10. (a) X. Zong, Y. Na, F. Wen, G. Ma, J. Yang, D. Wang, Y. Ma, M. Wang, L. Sun, C. Li, *Chem. Commun.* 2009, **30**, 4536; (b) S. Min, G. Lu, *J. Phys. Chem. C.* 2012, **116**, 25415.
11. (a) Y. Li, H. Wang, L. Xie, Y. Liang, G. Hong, H. Dai, *J. Am. Chem. Soc.* 2011, **133**, 7296; (b) Q. Xiang, J. Yu, M. Jaroniec, *J. Am. Chem. Soc.* 2012, **134**, 6575; (c) F. Meng, J. Li, S. K. Cushing, M. Zhi, N. Wu, *J. Am. Chem. Soc.* 2013, **135**, 10286; (d) K. Chang, Z. Mei, T. Wang, Q. Kang, S. Ouyang, J. Ye, *ACS Nano* 2014, **8**, 7078. (e) J. Xu, X. Cao, *Chem. Eng. J.* 2015, **260**, 642.
12. (a) Z. Bian, T. Tachikawa, T. Majima, *J. Phys. Chem. Lett.* 2012, **3**, 1422; (b) Z. Bian, T. Tachikawa, P. Zhang, M. Fujitsuka, T. Majima, *J. Am. Chem. Soc.* 2014, **136**, 458; (c) T. Tachikawa, P. Zhang, Z. Bian, T. Majima, *J. Mater. Chem. A* 2014, **2**, 3381; (d) Z. Bian, T. Tachikawa, P. Zhang, M. Fujitsuka, T. Majima, *Nat. Commun.* 2014, **5**:3038.
13. S. S. Chou, B. Kaehr, J. Kim, B. M. Foley, M. De, P. E. Hopkins, J. Huang, C. J. Brinker, V. P. Dravid, *Angew. Chem., Int. Ed.* 2013, **52**, 4160.
14. Y. Yu, S. Y. Huang, Y. Li, S. N. Steinmann, W. Yang, L. Cao, *Nano Lett.* 2014, **14**, 553.
15. (a) T. Tachikawa, S. Yamashita, T. Majima, *J. Am. Chem. Soc.* 2011, **133**, 7197; (b) J. Pan, G. Liu, G. Q. Lu, H. M. Cheng, *Angew. Chem., Int. Ed.* 2011, **50**, 2133;. (c) Z. Bian, T. Tachikawa, W. Kim, W. Choi, T. Majima, *J. Phys. Chem. C* 2012, **116**, 25444.

